Helium transport in the core and stochastic edge layer in LHD

Helium transport in the core and stochastic edge layer in LHD

K. Ida[1], M. Yoshinuma[1], M. Goto[1], O. Schmitz[2], S. Dai[1], A.Bader[2], M. Kobayashi[1], G. Kawamura[1], C.Moon[1], Y.Nakamura[1], and the LHD Experiment Group[1, 2]

[1] *National Institute for Fusion Science, Toki, Gifu 509-5292, Japan*
[2] *University of Wisconsin, Madison, U.S.A.*

(Dated: May 26, 2016)

Radial profiles of the density ratio of helium to hydrogen ions are measured using charge exchange spectroscopy with a two-wavelength spectrometer in the Large Helical Device. Helium transport at the last closed flux surface (LCFS) and stochastic magnetic field layer outside the LCFS as well as in the core plasma is studied for a wide range of helium fractions, i.e. from hydrogen-dominated plasmas up to helium-dominated plasmas. The helium density profile becomes more peaked and inward convection velocity increases in the hydrogen-dominant plasma, while it becomes flat or hollow and the convection velocity is in the outward direction in the helium-dominant plasmas. The density gradient of helium at the LCFS is twice that of hydrogen and becomes steeper as the hydrogen becomes more dominant.

PACS numbers: 52.55.Hc, 52.55.Fa, 52.50.Sw, 52.50.Gj

I. INTRODUCTION

Helium transport is one of the crucial issues in fusion plasmas, because the efficient exhaust of the helium ash produced by the fusion reaction is a crucial issue. The helium transport in the core plasma has been studied by using charge exchange spectroscopy in order to investigate whether the helium ash is accumulated in the plasma center [1–5]. The charge exchange spectroscopy was applied to the bulk and helium plasmas, and radial profiles of helium and bulk ions can be measured by subtracting the emission from the plasma periphery with beam modulation method [6–8]. The precise measurements of helium profiles provide the transport parameters, diffusion coefficient and convective velocity, in the plasma core.

It has been reported that the diffusion coefficient evaluated from the time evolution of helium density measured with charge exchange spectroscopy is comparable to the ion and electron thermal diffusivity and momentum diffusivity in TFTR tokamak [9]. The peaking factor is similar to the peaking factor of the electrons, i.e. the radial profiles of helium and the electrons have a similar radial shape[10]. However, in the fusion plasma, where the helium ash is produced by the deuterium-tritium reaction, the helium ash confinement time is dominated by the edge transport, recycling and edge pumping rate rather than the core transport [11]. High helium pumping efficiency is necessary for the plasma with enhanced confinement regime [2].

Therefore, the helium transport near the last closed flux surface (LCFS) would be more important than the helium transport in the core plasma. The helium transport at the LCFS and stochastic edge layer has not been studied sufficiently despite its importance [12]. In this paper, the helium density profiles measured with charge exchange spectroscopy up to the LCFS and even outside the LCFS are presented and the helium transport crossing the LCFS region as well as the transport in the core region are discussed.

II. HELIUM TRANSPORT IN THE CORE AND EDGE

Recently, a two-wavelength spectrometer for HeII and HI charge exchange lines has been installed in the Large Helical Device (LHD) for helium transport studies and radial profiles of helium and hydrogen density are measured near and outside the LCFS as well as in the core plasma [13]. This two-wavelength spectrometer gives simultaneous measurements of helium and hydrogen density profiles at exactly the same locations and provide the helium to hydrogen density ratio in the wide range of helium fractions. Since radial profiles of both helium and hydrogen density are measured, this spectrometer is useful to investigate the difference in transport between bulk ion and helium.

A. Relation of edge helium density ratio and influx ratio

In LHD, the width of the stochastic layer varies depending on vacuum magnetic axis position. In the outward shifted configuration ($R_{\rm ax}$ = 3.9 m), the stochastic layer near the plasma edge becomes wider than that in the inward shifted configuration ($R_{\rm ax}$ = 3.6 m). Figure 1 shows the time evolution and radial profiles of the ratio of helium density to hydrogen density in the inward shifted configuration with a vacuum magnetic axis of 3.6m and the outward shifted configuration with a vacuum magnetic axis of 3.9m. After the helium gas puff at t = 3.4 sec for $R_{\rm ax}$ = 3.6 m configuration and t = 3.9 sec for $R_{\rm ax}$ = 3.9 m configuration, the ratio of helium density to hydrogen density begins to increase.

In this experiment, the ratio of helium influx to hydrogen influx is evaluated from the intensity ratio of H_α (656.3 nm) to HeI (667.8nm) measured with passive spectroscopy using a collisional-radiative model [14]. The two lines in which the wavelength is close enough to be mea-

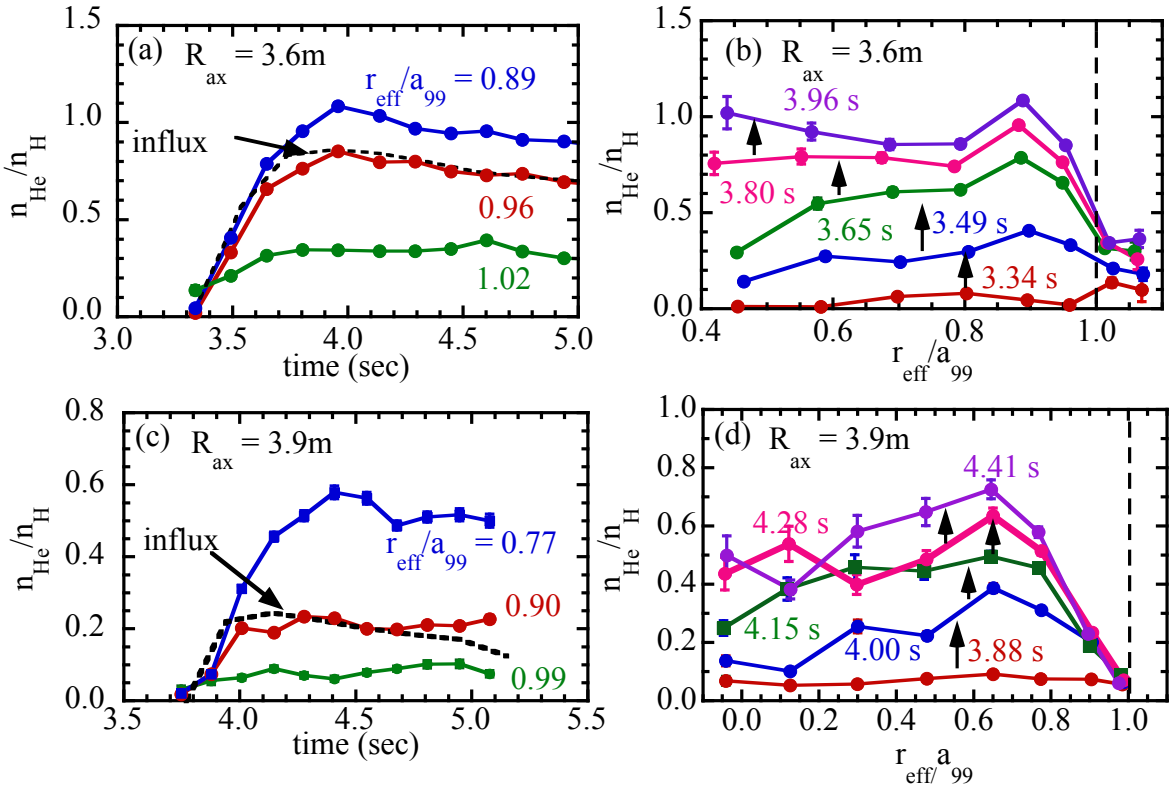

FIG. 1: (a) Time evolution and (b) radial profiles of helium to hydrogen ratio in the plasma with a vacuum magnetic axis of 3.6m and (c)(d) those in the plasma with a vacuum magnetic axis of 3.9m. The dashed lines indicate the location of LCFS.

sured simultaneously with one detector are selected to avoid the uncertainty of the relative sensitivity of spectrometer and detector for these two lines. The ratio of helium influx to hydrogen influx derived from the passive spectroscopy matches well to the ratio of helium density to hydrogen density derived from charge exchange spectroscopy near the plasma edge at $r_{\rm eff}/a_{99}$ =0.96 for $R_{\rm ax}$ = 3.6 m and $r_{\rm eff}/a_{99}$ =0.90 for $R_{\rm ax}$ = 3.9 m.

The radial profile of the density ratio of helium to hydrogen show the differences depending on the magnetic field configurations. In the inward configuration, the sharp increase of helium to hydrogen ratio is observed at the LCFS ($r_{\rm eff}/a_{99} = 1$). This observation clearly shows the better confinement of helium than that of hydrogen. If there is no difference in transport between helium and hydrogen, the ratio should be flat (constant in space). In the inward shifted configuration, the ratio of helium to hydrogen density begins to increase outside the LCFS and the sharp increase is observed at the LCFS. In the outward shifted configuration, the ratio of helium to hydrogen density begins to increase inside the LCFS and the increase of helium to hydrogen ratio inside the LCFS is gradual. Although the radial profiles of helium to hydrogen ratio are quite different between $R_{\rm ax}$ = 3.6 m and $R_{\rm ax}$ = 3.9 m configuration, the influx ratio is consistent with the density ratio at 90% or 95% of the normalized minor radius. It is interesting that the helium influx ratio agrees with the density ratio inside the LCFS and does not agree with the density ratio outside or at the LCFS for both inward ($R_{\rm ax}$ = 3.6 m) and outward shifted ($R_{\rm ax}$ = 3.9 m) configurations.

Figure 2 shows the relation between the ratio of helium influx to hydrogen influx and the ratio of helium density to hydrogen density near the edge at $r_{\rm eff}/a_{99} \sim$ 0.9. There is good agreement of these two ratios in a wide range of the ratio of helium to hydrogen (n_{He}/n_H) from 0.05 to 5 by two orders of magnitude. The fraction of helium is controlled by the helium gas puff. In the plasma of low fraction of helium, there is no helium gas puff and helium is fueled only by recycling. It should be noted that the electron temperature at $r_{\rm eff}/a_{99} \sim 0.9$ is a few hundred eV and much higher than the ionization potential of helium. The density ratio of helium to hydrogen at $r_{\rm eff}/a_{99} \sim 0.9$ is used as a monitor of the helium to hydrogen influx ratio in this paper.

B. Effect of helium fraction on transport in the plasma core and at the LCFS

Figure 3 shows radial profiles of electron temperature, electron density, hydrogen density, helium density, and

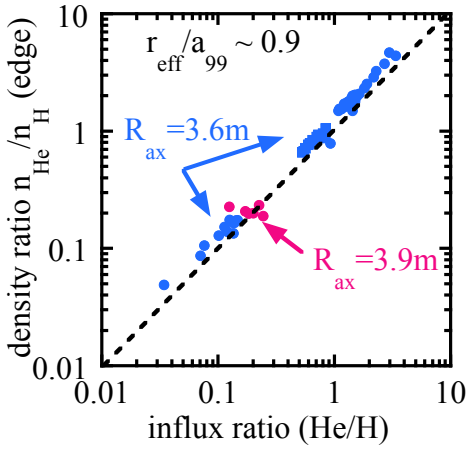

FIG. 2: Relation of the edge helium to hydrogen density ratio at $r_{\rm eff}/a_{99} \sim 0.9$ to the helium to hydrogen influx ratio derived from the intensity ratio of the two lines, H_α (656.3 nm) and HeI (667.8nm).

the ratio of helium to hydrogen density in the plasmas with weak and strong helium puff. It is interesting that the radial profiles of helium density to hydrogen density depends on the ratio of helium to hydrogen. The ratio of helium to hydrogen density is ~ 0.1 for the weak helium gas puff, while it is ~ 3 for the strong helium gas puff.

In the discharge with the hydrogen dominant plasma, the helium density profile is peaked and the hydrogen density profile is flat. Then the radial profile of the ratio of helium density to hydrogen density is also peaked. In contrast, in the discharge with the helium dominant plasma, the helium density profile is flat and the hydrogen density profile is peaked. Then the radial profile of the ratio of helium density to hydrogen density becomes hollow. When the ratio of helium to hydrogen density is low enough, the helium can be treated as an impurity. However, when the ratio of helium to hydrogen becomes large, the helium transport is governed by the electron transport rather than the impurity transport and hydrogen can be treated as an impurity. These observations show the density peaking of minority species (helium density peaking in the hydrogen dominant plasma and the hydrogen density peaking in the helium dominant plasma), regardless of the species.

Figure 4 shows the time evolution of radial profiles in the two discharges: one is the discharge with lower helium fraction and the other is the discharge with higher helium fraction. When the helium fraction is low, the helium density profile becomes more peaked in time during the discharge, as seen in Fig.4(a)(b)(c). The radial profiles of helium to hydrogen density ratio also become peaked and core helium fraction at $r_{\rm eff}/a_{99} = 0.44$ is twice the edge helium fraction at $r_{\rm eff}/a_{99} = 0.89$. Although

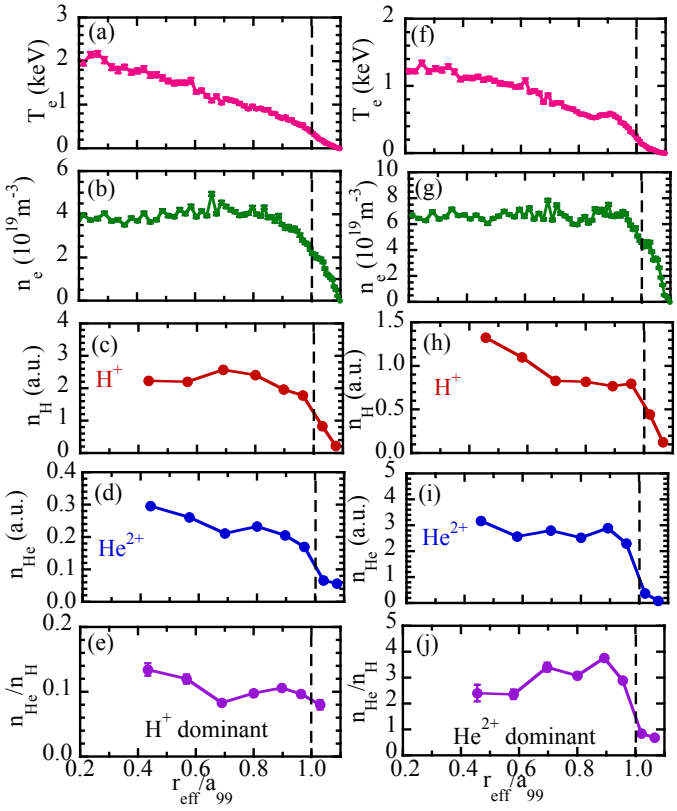

FIG. 3: Radial profiles of (a)(f) electron temperature (b)(g) electron density, and (c)(h) helium density (d)(i) hydrogen density (e)(j) ratio of helium to hydrogen density in the (a)-(e) hydrogen and (f)-(j) helium dominant plasmas. The dashed lines indicate the location of LCFS.

the fraction of helium itself is small, the time evolution of the radial profile of the helium to hydrogen density ratio clearly shows the impurity accumulation [15]. In contrast, in the discharge with higher helium fraction by additional helium gas puff, the helium density profile becomes hollow in time. The radial profiles of helium to hydrogen density ratio also become hollow, and core helium fraction at $r_{\rm eff}/a_{99} = 0.44$ is even lower than the edge helium fraction at $r_{\rm eff}/a_{99} = 0.89$. This observation suggests that the sign of the convective velocity is sensitive to the fraction of helium and can be reversed. In the lower helium fraction, the convection velocity is negative (inward), while it becomes positive (outward) in the higher helium fraction.

This experiment clearly shows that the radial profile of helium to hydrogen ratio in the core is not always flat and becomes peaked or hollow depending on the fraction of helium, and does not depend on the plasma density, which strongly suggests that the helium transport differs from that of hydrogen. In the diffusion and convection model of impurity transport, the impurity radial flux can be expressed as $-D\partial n_I/\partial r + v n_I$ and $v = -2c_v Dr/a^2$, where D is diffusion coefficient and c_v is peaking fac-

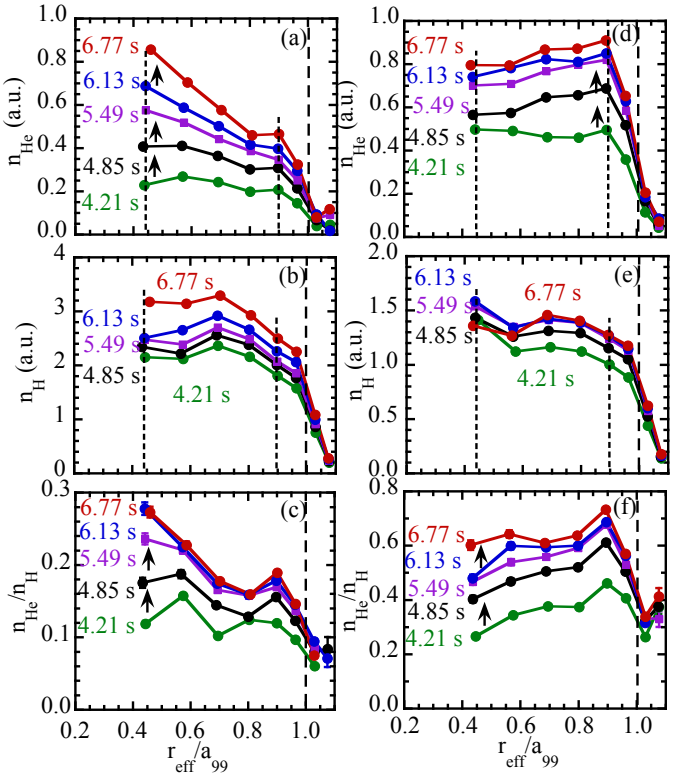

FIG. 4: Radial profiles of (a)(d) helium density (b)(e) hydrogen density, and (c)(f) ratio of helium to hydrogen density helium density in the (a)-(c) low helium fraction and (d)-(f) high helium fraction. The dashed lines indicate the location of LCFS. The density gradients between the two dotted lines are used to evaluate the peaking factors.

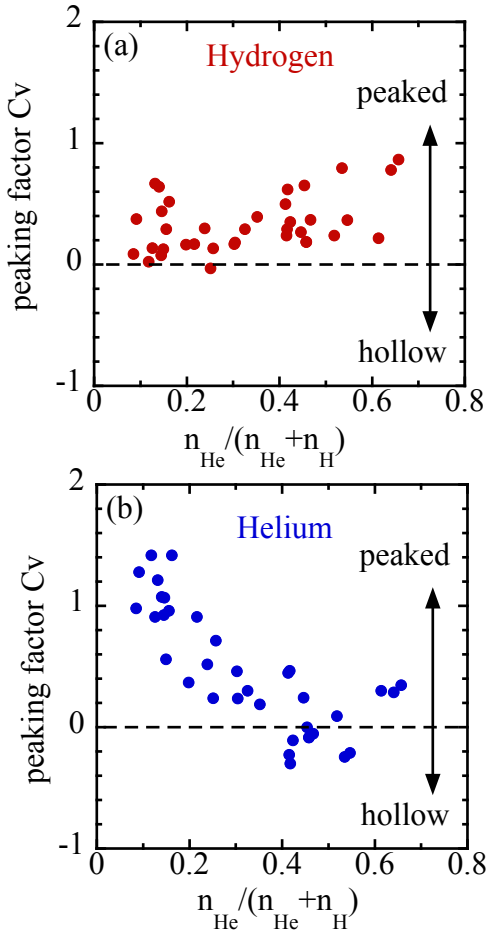

FIG. 5: Peaking factor c_v of (a) hydrogen and (b)helium ions as a function of edge helium fraction.

tor. In the steady state, the impurity density becomes $n_I \propto \exp(-c_v r^2/a^2)$. The peaking factor c_v can be evaluated from the ratio of impurity density at two different locations of $r_{\rm eff}/a_{99} = 0.44$ and 0.89 in the late phase of the discharge ($t > 6$ s) where the density profile reaches the steady-state determined by the diffusion and convective velocity discussed above.

Figure 5 shows the peaking factor of hydrogen and helium ions as a function of the helium fraction near the plasma edge of $r_{\rm eff}/a_{99} \sim 0.9$. As the helium fraction is increased the peaking factor of helium significantly decreases from 1.5 (peaked) to -0.3 (hollow), while the peaking factor of hydrogen shows a slight increase. These results show that the helium impurity is peaked, but there is no peaking of helium ions in the helium dominant plasma, because the radial profiles of helium ions are determined by the electron particle transport rather than the impurity transport. These results clearly show the difference between bulk transport and impurity transport. It is interesting that even hydrogen tends to be slightly peaked when the fraction of hydrogen decreases and hydrogen is treated as an impurity species.

The other important finding in this experiment is that the helium to hydrogen density ratio outside the LCFS ($r_{\rm eff}/a_{99} > 1$) is much smaller than that in the core, which indicates the difference of confinement at LCFS between helium and hydrogen. The scale lengths of hydrogen and helium density at the LCFS are evaluated in order to discuss the difference in confinement characteristics between helium and hydrogen at LCFS. Figure 6 shows the inverse of hydrogen and helium density scale length L_n normalized by minor radius a. Here, the helium density scale length L_n is defined by $n_i(\partial n_i/\partial r_{\rm eff})^{-1}$ and evaluated from the density ratio at $r_{\rm eff}/a_{99} = 0.96$ and 1.03.

The helium density gradient a/L_n is 15 - 20 and is almost twice the hydrogen density gradient. This large difference in the gradient can not be explained with differences in the source profile (as will be shown below by EMC3-EIRENE calculations) and must be due to a larger inward drift of Helium leading to a better confinement of Helium in comparison to Hydrogen. Both density gradients increase as the helium fraction is de-

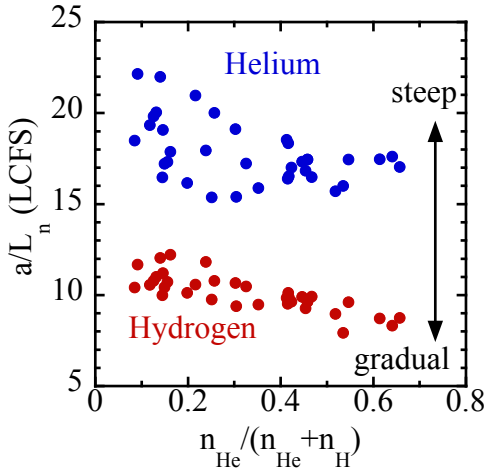

FIG. 6: Normalized density gradient (inverse of scale length of helium and hydrogen density normalized by a minor radius) evaluated from the density ratio at $r_{\rm eff}/a_{99} = 0.96$ and 1.03 as a function of edge helium fraction.

creased. The confinement of helium at LCFS becomes better as the influx of helium and edge helium density decrease. The transport of helium observed in the core and at the LCFS are not desirable characteristics from the point of helium exhaust, because as the helium fraction decreases the helium density becomes peaked and confinement at the LCFS becomes better.

III. COMPARISON OF HELIUM FRACTION BETWEEN OBSERVATION AND EMC3-EIRENE SIMULATION

In the EMC3-EIRENE simulation, the so-called impurity shielding is predicted at higher edge electron density because the outward directed flow from impurity-ion friction is larger than the inward directed flow from thermal gradients [16]. In this section, this impurity shield effect is discussed by comparing the helium density profile measured and predicted by EMC3-EIRENE simulation outside the LCFS. Figure 7 shows comparisons between the experiments and the EMC3-EIRENE simulations for the configuration of $R_{\rm ax} = 3.60$ m for the low and high density cases. The location of the LCFS is indicated with dashed lines. The electron temperature and electron density at the LCFS is 0.2 - 0.3 keV and 1.4 and 4 $\times 10^{19}$ m^{-3}. In the experiments, it is shown that the He^{2+} density gradient becomes steeper for the high density case outside the LCFS.

In contrast, the EMC3-EIRENE simulation predicts flat profile just outside the LCFS. The location of the sharp decrease of fully ionized helium He^{2+} density appears at $R > 4.65$ m more outside than that in experiment , and the He^{1+} density increases sharply due to the drop of electron temperature. The sharp decrease of helium density observed in the high density plasma is not due to the drop of electron temperature. There is a small peak in He^{2+} around $R = 4.65$ m in the high density case, which is not observed in experiment. However, it should be noted that the charge exchange spectroscopy does not have enough spatial resolution to detect this small peak at $R = 4.65$ m outside the LCFS, if any. In the simulation, it is found that there is no remarkable screening effect even in the high density case, where the total He density (He^{1+} + He^{2+}) is still higher around the LCFS than at the periphery ($R \sim 4.8$ m). This is in contrast to previous results for carbon and iron impurity, in which the impurity is effectively screened in the edge stochastic region, as has been in good agreement with the behavior of impurity emission in experiments [17, 18].

The slight increase in He^{1+} around $R = 4.8$ m in the high density case (Fig.7 (h)) as compared to the low den-

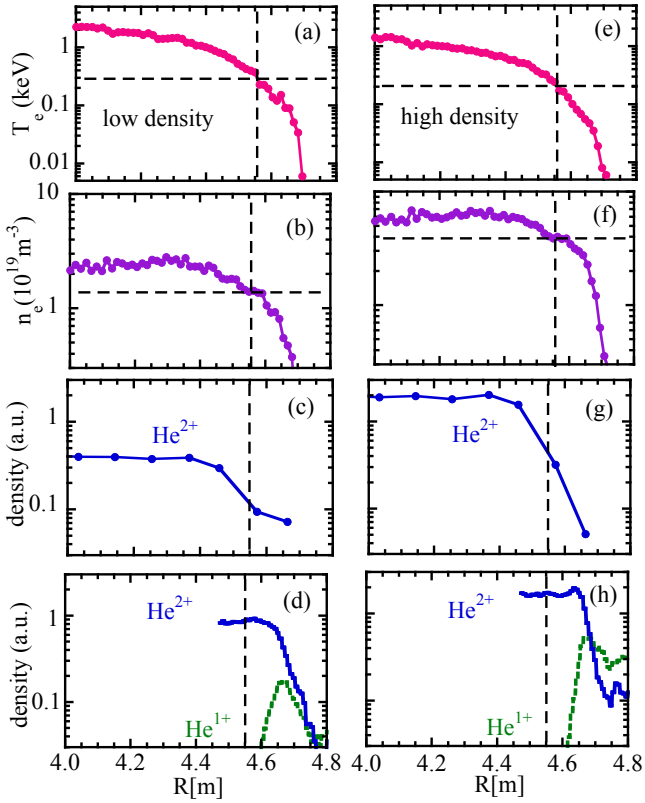

FIG. 7: Radial profiles of (a)(e) electron temperature (b)(f) electron density, (c)(g) helium density measured, and (d)(h) helium densities calculated with EMC3-EIRENE.

sity case (Fig.7 (d)) might reflect a signature of change in impurity transport regime from thermal force dominant (inward impurity flux) to friction force dominant (outward impurity flux, i.e., screening). But the effect is still small as compared to the previous analysis of carbon and iron. There are two reasons for this result: One reason is the higher ionization potential of He (24.6 eV) than those of carbon (11.3 eV) and iron (7.9 eV), which thus allows He to penetrate so deeply that it feels less friction force in the edge region to screen the impurity. The other reason is the thinner stochastic layer of the present configuration ($R_{\rm ax}$ = 3.60 m), which has less screening effect compared to the thicker stochastic layer as investigated in the previous analyses. Additionally, there are still several unknown parameters in the simulation, which can affect the resulting He distribution: the location and injection energy of the He source, reflection coefficient of He (i.e. recycling rate) at the first wall, and parallel and perpendicular transport coefficients of He.

In the present simulation, the He source is located at the divertor plates assuming dominant recycling flux there compared to the flux at the gas puff nozzle. The ejection energy is 0.05 eV and 1 % of plasma particle flux is assumed for He flux. The perpendicular diffusion coefficients of He and main ion are set to the same value (0.40 m^2/s), while the parallel transport coefficient is set to the default values of the classical momentum transport formulation [17]. However, it has been shown that the selection of these parameters can substantially affect the impurity density distribution of carbon [19]. A systematic parameter scan study is, therefore, necessary for the He case as well, in order to investigate the reasons for the difference between the simulation and experiments as observed in Fig.7.

From the experimental results in Fig.7, we have found that across the LCFS there is a large change of He^{2+} density profiles, which is not reproduced in the computation with the edge transport model implemented in the present version. These results indicate an importance of transport mechanism, such as radial electric field, neoclassical effects, etc., which are not present in the simulation. For example, the edge radial electric field changes its sign from positive to negative as the edge density and collisionality increase [20] and the radial electric field has large variation in space especially at the LCFS [21]. In experiment, it was found that the impurity transport is very sensitive to the sign of the radial electric field, i.e, a positive radial electric field has a significant role to change the sign of convection from inward to outward and prevent radial collapse even with a large amount of impurity gas puff [22]. Convection velocity becomes inward for a negative radial electric field, while it becomes outward for a positive radial electric field. 4Therefore, the radial electric field and its effect on impurity transport should be included In EMC3-EIRENE simulationsin order to compare the radial profile of helium density with experimental results.

In conclusion, the helium transport and hydrogen transport are studied near the LCFS as well as in the plasma core region using the bulk charge exchange spectroscopy. The influx ratio derived from HeI and HI agrees with the density ratio inside the LCFS at $r_{\rm eff}/a_{99} \sim 0.9$ in a wide range of the ratio of helium to hydrogen density of $0.05 \sim 5$. In the core region, the peaking factor cv of helium is positive (inward convection) at low helium fraction ($n_{He}/n_H < 0.2$), while it becomes negative (outward convection) at higher helium fraction ($n_{He}/n_H > 0.4$). The reversal of convection observed is not predicted by neoclassical transport theory. The helium density gradient is twice the hydrogen density gradient at the LCFS. Both density gradients decrease as the edge electron density is increased. A comparison between measurements and EMC3-EIRENE simulations is performed outside the LCFS. In the experiments, the He^{2+} density gradient becomes steeper for the high density case outside the LCFS, which is not predicted by EMC3-EIRENE simulation.

The author would like to thank the technical staff of the Large Helical Device for their support of these experiments. This work is partly supported by a Grant-in-Aid for Scientific Research of Japan Society for the Promotion of Science (JSPS) (No. 15H02336). This work is also partly supported by the National Institute for Fusion Science grant administrative budget (NIFS10ULHH021).

References

[1] Fonck R.J and Hulse R, Finkenthal M 1984 *Phys. Rev. Lett.* **52** 530.
[2] Hillis D.L *et al* 1992 *J. Nucl. Mater.* **196-198** 35.
[3] Wade M.R *et al* 1995 *J. Nucl. Mater.* **220-222** 178.
[4] Sakasai A *et al* 1995 *J. Nucl. Mater.* **220-222** 405.
[5] Hogan J *et al* 1997 *J. Nucl. Mater.* **241-243** 68.
[6] Busche E, Euringer H, and Jaspers R, 1997 *Plasma Phys. Control. Fusion* **39** 1327.
[7] Pütterich T, Wolfrum E, Dux R, and Maggi C, 2009 *Phys. Rev. Lett.* **102** 025001.
[8] Grierson B.A, *et al* 2012 *Rev. Sci. Instrum.* **83** 10D529.
[9] Synakowski E.J *et al* 1990 *Phys. Rev. Lett* **65** 2255.
[10] Wade M.R *et al* 1995 *Phys. Plasmas* **2** 2357.
[11] Synakowski E.J *et al* 1995 *Phys. Rev. Lett* **75** 3689.
[12] Peng L.L *et al* 1997 *J. Nucl. Mater.* **241-243** 883.
[13] Ida K *et al* 2015 *Rev Sci Instrum.* **86** 123514.
[14] Goto M, Sawada K, and Fujimoto T, 2002 *Phys. Plasmas* **9** 4316.
[15] Nakamura Y *et al* 2003 *Nucl. Fusion* **43** 219.
[16] Kobayashi M *et al* 2013 *Nucl. Fusion* **53** 093032.
[17] Kobayashi M *et al* 2013 *Nucl. Fusion* **53** 033011.
[18] Morita S *et al* 2013 *Nucl. Fusion* **53** 093017.

[19] Dai S *et al* EMC3-EIRENE modeling of edge impurity transport in the stochastic layer of LHD compared with EUV emission measurements 2016 *Nucl. Fusion* submitted.
[20] Ida K *et al* 2001 *Phys. Rev. Lett.* **86** 5297.
[21] Kamiya K *et al* 2013 *Nucl. Fusion* **53** 013003.
[22] Ida K *et al* 2005 *Nucl. Fusion* **45** 391.